Reversible Sequence-Dependent DNA Coacervation with an Azobenzene Intercalator

Yunzhe Li, Julie Pham, Mathieu Morel, Damien Baigl, and Sergii Rudiuk*

Cite This: https://doi.org/10.1021/acs.langmuir.5c04489

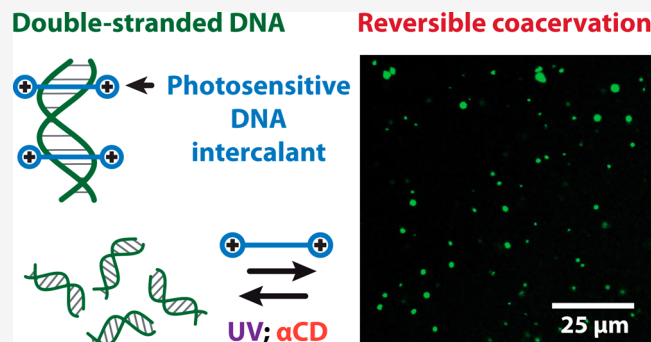Read Online

| ACCESS | Metrics & More | Article Recommendations | Supporting Information |

ABSTRACT: Based on electrostatic interactions and entropic gains from counterion release, DNA coacervates constitute an exciting example of associative assemblies due to high local DNA concentrations and their applications in therapeutics, biomimicry, and biosensing. Because charge density is not affected by DNA sequence, resulting coacervates are intrinsically nonspecific to the nucleobase composition of DNA. Here, we report that using an azobenzene-based DNA binder, AzodiGua, able to intercalate between DNA base pairs, can bring sequence sensitivity to DNA coacervation. We show that different amounts of AzodiGua are necessary to induce coacervation as a function of the double- or single-stranded nature of DNA, the fraction and distribution of GC base pairs a per double-stranded DNA oligonucleotides. In addition, resulting coacervates are shown to be reversibly photosensitive via *trans/cis* isomerization of AzodiGua's azobenzene moiety. Due to the lower efficiency of the *cis*-isomer for DNA coacervation, coacervates can be dissolved by UV illumination and reformed back by blue light illumination. Interestingly, selective sequestration of the *trans*-AzodiGua by α-cyclodextrin allows us to achieve a reversed-photocontrol regime, under which coacervates are favored under UV illumination.

1. INTRODUCTION

Coacervation refers to associative liquid–liquid phase separation in polyelectrolyte solutions.[1,2] Typically observed in interpolyelectrolyte complexes, a similar process occurs upon electrostatic interactions of a polyelectrolyte with oppositely charged proteins or even small molecules.[3] Nucleic acid and/or protein coacervates are used to mimic natural membrane-less organelles, such as nucleoli and stress granules, which compartmentalize biochemical reactions without needing a lipid membrane,[4] and are able to affect cell behavior by sequestering cellular factors.[5] Coacervates have also been applied for immobilizing enzymatic cascades,[6] increasing the local concentration of DNA-based biosensors,[7] performing nonenzymatic DNA ligation,[8] as well as for drug[9,10] and gene or mRNA vaccine delivery,[11−14] making reversible coacervation promising for the efficient release of the loaded components. Various approaches have thus been used for the reversible formation and dissolution of DNA coacervates, based on pH-,[14,15] temperature-,[15] or redox[14]-responsive coacervation agents. Due to its tunability and spatiotemporal resolution, photocontrol represents a promising opportunity for the actuation of DNA coacervates and liberation of DNA or other sequestered molecules on demand. One approach consists of introducing a photoswitchable arylazopyrazole moiety directly into DNA before its coacervation with polylysine.[16] Another approach is based on using a positively charged photosensitive surfactant, AzoTAB, for DNA coac-

ervation.[8,17,18] At micromolar concentrations of DNA, this molecule was used for photocontrol of DNA compaction[19,20] and gene expression.[21,22] However, at higher DNA concentrations, it was found to induce the formation of DNA coacervate microdroplets, which were also shown to be photosensitive: the resulting coacervates could efficiently dissolve and reform upon UV and blue light illumination, respectively.[17]

The combination of photosensitivity with sequence dependency can represent significant interest for sequestration or purification of DNA molecules by their sequence. A number of hybridization-based, and thus intrinsically sequence-specific, DNA microdroplets formed by liquid–liquid phase separation have recently been described.[23−26] However, even though sequence-dependent coacervation could be achieved for polypeptides[27] and proteins[28,29] by controlling the distribution of charged amino acids, due to homogeneous charge distribution along the DNA molecule, its electrostatically based coacervation is typically nonspecific to the DNA
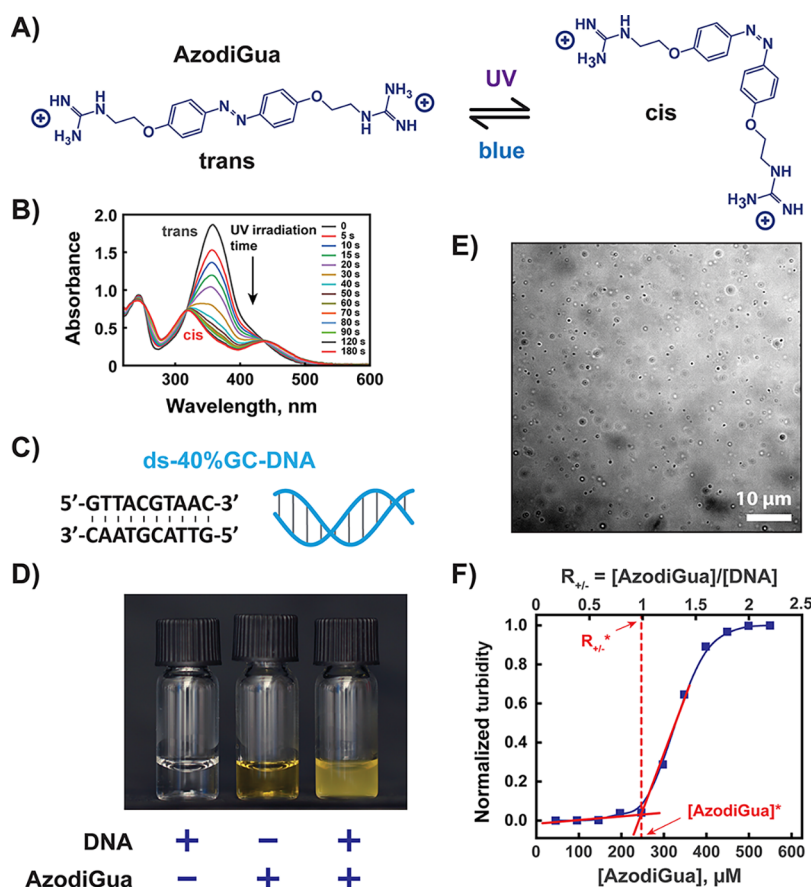
A

Figure 1. Experimental system and characterization of DNA coacervates. (A) Chemical structure and photoisomerization of AzodiGua (UV: 365 nm; blue: 440 nm). (B) Absorbance spectra of *trans*-AzodiGua at increasing UV irradiation times (365 nm, 0.35 mW·cm^{-2}); [AzodiGua] = 50 μM. (C) Scheme and sequence of self-complementary 10-bp DNA having 40% GC base pairs (ds-40%GC-DNA). (D) Images of transparent solutions of ds-40%GC-DNA alone and AzodiGua alone (300 μM), and a turbid mixture of both components (15 min after the mixing). The volume of the solutions is 400 μL, and the vial diameter is 11.6 mm. (E) Optical transmission microscopy image of DNA coacervates from the right solution in (D). (F) Typical turbidity curve obtained by measuring the absorbance at 700 nm of the solution/suspension obtained by mixing ds-40%GC-DNA with increasing amounts of AzodiGua. [AzodiGua]* and $R_\pm$* are defined, respectively, as the characteristic AzodiGua concentration and the AzodiGua/DNA charge ratio at the onset of turbidity increase. All experiments are performed in 10 mM Tris/HCl, pH 7.4; [ds-40%GC-DNA] = 500 μM in charge.

sequence and structure. The only example of sequence- and structure-dependent DNA coacervation was reported by Tirell and co-workers.[30] By investigating the interactions of DNA oligonucleotides with polylysines, it was found that while single-stranded (ss) DNAs formed spherical coacervate microdroplets, double-stranded (ds) DNAs produced solid aggregates. In addition, ss-DNAs of different sequences showed nonhomogeneous effects on the phase behavior of their complexes with polylysine. This work clearly demonstrated differences in the coacervation of ss- and ds-DNA oligonucleotides, but the observed effect of sequence was explained by the formation of secondary structures through intra- or interoligonucleotide hybridization leading to the formation of ds-DNA fragments, rather than the effect of the DNA sequence itself.

Our strategy to achieve sequence-dependent electrostatic coacervation of DNA involved implementing positively charged DNA intercalators, as the inclusion of flat aromatic molecules between DNA base pairs is known to be sensitive to the sequence of DNA[31,32] due to differential interactions with AT and GC base pairs. Here, we used a photosensitive dicationic DNA intercalator, AzodiGua, for photosensitive and sequence-dependent DNA coacervation. Previously, we have

demonstrated that this molecule was not only able to intercalate into the DNA double helix[33,34] but could also bind to DNA nucleotides through a combination of electrostatic interactions, $\pi-\pi$ stacking, and H-bonding.[35,36] Here, we show for the first time that AzodiGua can induce liquid−liquid phase separation of DNA in a structure- and sequence-dependent manner. For this purpose, we compare DNA/AzodiGua coacervation for ss- and ds-DNA of different sequences (%GC) and demonstrate two efficient approaches for making this process reversible: by photoinduced *trans*−*cis* isomerization of the azobenzene moiety and by competitive host−guest binding of the intercalator to α-cyclodextrin (αCD).

2. MATERIALS AND METHODS

2.1. Materials. All oligonucleotides, Trizma base, Trizma hydrochloride, sodium chloride (NaCl), αCD, dodecyltrimethylammonium bromide (DTAB), and sodium dodecyl sulfate (SDS) were purchased from Sigma/Aldrich. AzodiGua was synthesized by Novalix. Deionized MQ water (Millipore, 18 MΩ·cm) was used for all experiments. All oligonucleotides were purchased in the form of solutions in MQ water at a 500 μM strand concentration (5 mM in nucleobases). For all experiments, the oligonucleotides were used without any supplementary heat treatment: short 10 bases (10b) self-
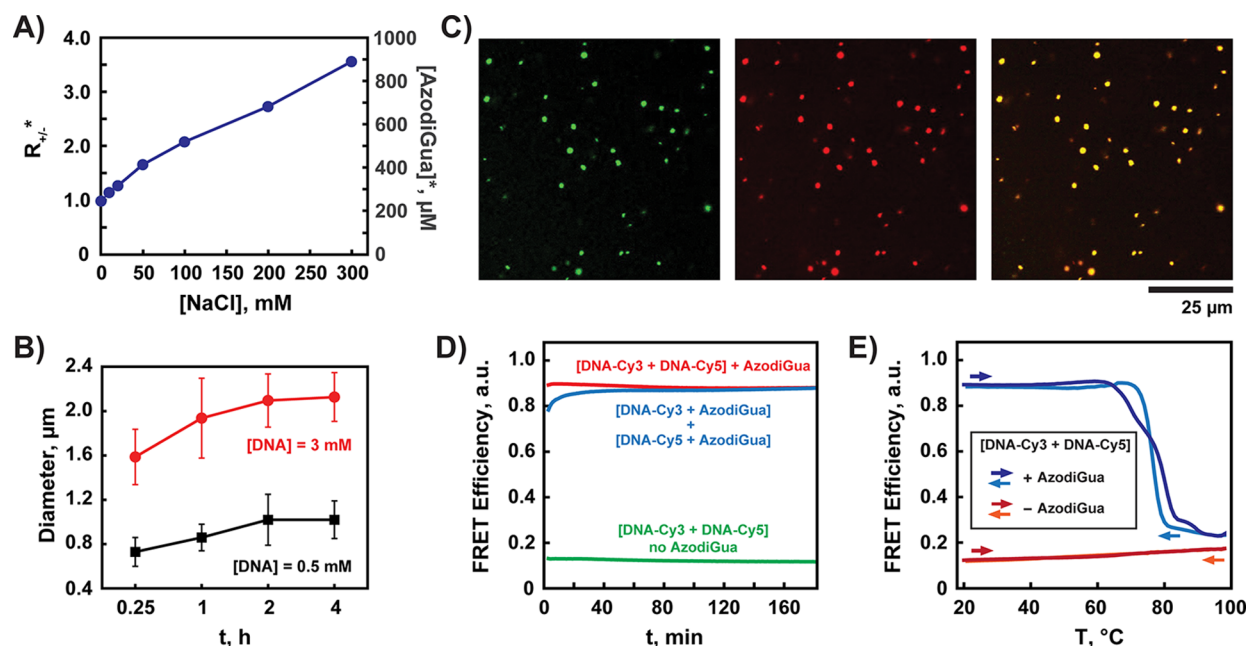
Figure 2. Physicochemical properties of DNA-AzodiGua coacervates. (A) Characteristic AzodiGua concentration ($[AzodiGua]^*$) and AzodiGua/ DNA charge ratio ($R_{\pm}^*$) for 500 μM of ds-40%GC-DNA as a function of NaCl concentration. (B) Evolution of size measured by optical transmission microscopy for coacervate microdroplets formed with 500 μM or 3 mM (in phosphates) of ds-40%GC-DNA upon adding charge ratio $R_{\pm}$ = 1.2 of AzodiGua. (C) Confocal fluorescence microscopy observation of coacervates formed by adding AzodiGua to a mixture of two different ds-40%GC-DNAs: one labeled with Cy3 and another one with Cy5. Left: green, Cy3 channel (λ_{Ex} = 543 nm; λ_{Em} = 582/35 nm); middle: red, Cy5 channel (λ_{Ex} = 633 nm; λ_{Em} = 726/143 nm); right: composite image. (D) Evolution with time of the FRET efficiency for a mixture of ds-40%GC-DNAs labeled with Cy3 and Cy5 (250 μM of each) with (red) and without (green) AzodiGua ($R_{\pm}$ = 1.2). Blue curve represents the FRET efficiency for separately prepared and mixed (at t = 0) coacervates of ds-40%GC-DNA-Cy3 and ds-40%GC'-DNA-Cy5. The names of DNA are simplified to DNA-Cy3 and DNA-Cy5, respectively. (E) FRET efficiency as a function of temperature for a mixture of ds-40%GC-DNAs labeled with Cy3 and Cy5 (250 μM each) before (red) and after (blue) adding AzodiGua ($R_{\pm}$ = 1.2). The arrows indicate heating/cooling directions. For FRET measurement, λ_{Ex} = 520 nm, λ_{Em}(donor) = 550 nm, and λ_{Em}(acceptor) = 682 nm. All experiments are performed in Tris/HCl buffer, pH 7.4.

complementary oligonucleotides formed ds-DNA upon addition of Tris/HCl buffer, NaCl, and/or AzodiGua.

2.2. UV Spectroscopic Studies. The absorption spectra of AzodiGua (Figure 1B) were recorded with an Eppendorf BioSpectrometer. For the *trans—cis* photoisomerization study, the samples were irradiated for the necessary time with a UV lamp at 365 nm (Vilbert Lormat, 6 W) over a distance of 4–6 cm (0.35 mW·cm^{-2}) before recording the absorbance spectra in the range of 220–600 nm. The process was repeated until a *cis*-rich photostationary state was reached.

2.3. Preparation of Coacervates. Coacervate microdroplets were produced at room temperature by mixing aqueous stock solutions to give final concentrations [DNA] = 500 μM (in nucleobases) and the necessary AzodiGua concentrations in 10 mM Tris/HCl buffer (pH 7.4). Further analysis of the coacervates was performed after incubation at room temperature for ca. 15 min, unless otherwise specified.

2.4. Microscopy Observations. Coacervate microdroplet solutions were deposited on glass slides and directly imaged with an optical microscope (Observer D1, Zeiss) equipped with a 100× oil immersion lens (Zeiss).

2.5. Turbidity Measurements. Turbidities of the samples were monitored by directly measuring their absorbance (with an Eppendorf BioSpectrometer) at 700 nm, a wavelength at which neither DNA nor AzodiGua absorbs light (Supplementary Figure S1). To facilitate comparison of different samples, the turbidity curves were normalized by the maximum value of the plateau.

2.6. Photocontrol of Coacervates. In situ UV irradiation of DNA/AzodiGua coacervates was performed using a UV lamp at 365 nm (Vilbert Lormat, 6 W) at 4–6 cm distance (0.35 mW·cm^{-2}). For blue light illumination, a cool LED (precisExcite) equipped with an optical fiber (112 mW·cm^{-2}) was used. Turbidity measurements and

optical microscopy observations of the samples were performed after each illumination step.

2.7. Confocal Observations. Solutions of mixed coacervates formed with two different ds-40%GC-DNAs labeled, respectively, with Cy3 and Cy5 fluorophores at their 5' termini (Supplementary Table S1) were deposited on glass slides. The samples were then observed in solution using an LSM-710 confocal microscope (Zeiss) equipped with a Plan-Apochromat 63×/1.40 Oil DIC M27 oil immersion lens. Cy3 channel: λ_{Ex} = 543 nm and λ_{Em} = 582/35 nm; Cy5 channel: λ_{Ex} = 633 nm and λ_{Em} = 726/143 nm.

2.8. FRET Measurements. Solutions of mixed coacervates formed with two different ds-40%GC-DNAs, labeled, respectively, with a Cy3 energy donor (D) and a Cy5 energy acceptor (A), were introduced into 96-well plates, and the fluorescence intensities of the donor (I_D) and acceptor (I_A) fluorophores were measured using QuantStudio 5 applied biosystems qPCR (Thermo Fisher Scientific), either under conditions of constant incubation at 25 °C or at a temperature ramp from 25 to 98 °C with a heating rate of 1 °C per minute. The FRET efficiency (E_{FRET}) was then calculated according to the equation $E_{FRET} = I_A/(I_A + I_D)$.

2.9. Calculation of the Gibbs Free Energy of Hybridization. All ΔG values for different ds-40%GC-DNAs were calculated using a self-dimer function in an online oligo analyzer on the Integrated DNA technologies (IDT) website: https://eu.idtdna.com/calc/analyzer

3. RESULTS AND DISCUSSION

First, we characterized the photoinduced *trans—cis* isomerization of AzodiGua (Figure 1A). In accordance to previous data, UV irradiation (365 nm, 0.35 mW·cm^{-2}) of *trans*-AzodiGua (50 μM) led to a gradual decrease in the absorbance band at 360 nm corresponding to the *trans*-isomer and the appearance of two new bands at 320 and 440 nm attributed to

the *cis*-isomer (Figure 1B).[33] In these conditions, a photostationary state was achieved after 2 min of irradiation. We then investigated coacervate formation for a 10-base pair (bp) ds-DNA formed by a self-complementary single strand containing 40% GC base pairs (referred to as ds-40%GC-DNA; Figure 1C) upon the addition of trans-AzodiGua. Mixing clear solutions of ds-40%GC-DNA (500 μM in charge) with 300 μM dicationic AzodiGua (600 μM in charge) produced, within seconds, a marked increase in turbidity (Figure 1D) and the appearance of micrometric spherical objects under optical microscopy (Figure 1E), which we can interpret as droplets. We attribute this behavior to the electrostatic attraction between AzodiGua and the DNA oligonucleotide leading to their coacervation. Such an attractive behavior has previously been observed for AzodiGua with other nucleotides, such as GMP[35] and ATP,[36] but those systems yielded solid-like assemblies, such as crystals or aggregates. In contrast, no aggregation was observed in our system. Instead, the spherical morphology of the objects formed here was consistent with liquid−liquid phase separation, i.e., coacervation. This mechanism is analogous to the findings of Martin et al.,[17] who reported coacervate formation at high oligonucleotide concentrations with AzoTAB, whereas the same molecule induced DNA compaction at low DNA concentrations.[37−39] Taken together, these observations lead us to conclude that coacervation in our system results from AzodiGua-mediated electrostatic attractions between oligonucleotides combined with the elevated oligonucleotide concentration.

To quantify the turbidity increase, the absorbance of the samples was measured at 700 nm, the wavelength at which both DNA and AzodiGua do not absorb the light directly (Figure S1). In the absence of light-absorbing chromophores, the increase in absorbance can be attributed to the amount of light scattered by coacervate microdroplets. We thus monitored the formation of coacervates by measuring the solution turbidity measured by its absorbance at 700 nm. A typical normalized turbidity curve for ds-40%GC-DNA as a function of the *trans*-AzodiGua concentration is shown in the Figure 1F. At low concentrations of AzodiGua, the turbidity stayed at zero. Upon further increase in [AzodiGua], the turbidity increased rapidly before reaching a plateau. Because the height of the plateau was found to depend on the DNA concentration and ionic strength of the solutions, we systematically normalized all turbidity curves by the maximum value corresponding to the plateau. From the turbidity curves, we then defined a characteristic AzodiGua concentration, noted as [AzodiGua]*, and the corresponding characteristic AzodiGua/DNA charge ratio ($R_\pm$*) at the onset of turbidity increase. These values were used for comparing the coacervation efficiency of different DNAs with different coacervation agents. For ds-40%GC-DNA, [AzodiGua]* was found to be 250 μM ($R_\pm$* = 1).

We then characterized the obtained DNA-AzodiGua coacervates. First, coacervation of ds-40%GC-DNA with *trans*-AzodiGua was studied at different ionic strengths of the solutions. We found that increasing [NaCl] from 0 to 300 mM (in 10 mM Tris/HCl buffer pH 7.4) led to the increase of [AzodiGua]* from 250 to 890 μM ($R_\pm$* from 1 to 3.6) (Figure 2A and Supplementary Figure S2), which confirms that DNA coacervation is based on electrostatic interactions between its phosphate groups and guanidinium functions of the AzodiGua. We then fixed the charge ratio $R_\pm$ to 1.2 and analyzed the stability of the DNA-AzodiGua coacervates by measuring from

transmission optical microscopy images the size of the observed microdroplets and its evolution with time. For 500 μM DNA, the size gradually increased during the first 2 h of incubation at room temperature from 0.7 ± 0.1 to 1.0 ± 0.2 μm (Figure 2B). When a higher concentration of DNA was used (3 mM), the size of the microdroplets became twice as big (1.6 ± 0.3 μm), and it also evolved during the 2 h of observation up to 2.1 ± 0.2 μm. In both cases, steady-state size was achieved after around 2 h and no size evolution was observed after an additional 2 h of incubation. To understand the origin of the stability of the microdroplets, we estimated whether they carried a residual charge by observing the interaction of the microdroplets prepared with a slight excess of AzoDiGua ($R_\pm$ = 1.2) with two kinds of charged surfactants, a cationic one (DTAB) and a negative one (SDS). It was found that, in contrast to DTAB, adding SDS induced the aggregation of droplets (Figure S3), which indirectly indicated a net positive charge of the coacervates, showing that the excess of AzoDiGua contributed to the overcharging of the droplets.

To analyze the thermal stability of the coacervates, FRET measurements were performed for coacervates obtained by adding *trans*-AzodiGua to a mixture of two different ds-40% GC-DNAs labeled with Cy3 and Cy5 and abbreviated as ds-40%GC-DNA-Cy3 and ds-40%GC′-DNA-Cy5, respectively (Supplementary Table S1). Confocal fluorescence microscopy of the resulting coacervates (Figure 2C and Supporting Information, Figure S4) showed colocalization of both fluorophores in all microdroplets, with a FRET efficiency of 0.9 stable in time (Figure 2D, red curve), confirming the formation of coacervates containing both DNAs. By following the FRET of this sample upon increasing the temperature, a steep decrease in the FRET efficiency from 0.9 to 0.2 was observed at around T = 80 °C (Figure 2E). Upon cooling down this solution, the FRET increased back to 0.9 at the same temperature, showing a fully reversible dissolution of the coacervates at high temperatures. This shows that DNA/AzodiGua coacervates are stable not only in time but also in a wide temperature range.

We then investigated the mixing of different coacervate microdroplets. For this purpose, coacervates of ds-40%GC-DNA-Cy3 and ds-40%GC′-DNA-Cy5 were formed separately by adding $R_\pm$ = 1.2 of *trans*-AzodiGua to each DNA. Then, both samples were mixed and their interaction was followed by FRET measurements (Figure 2D, blue curve). Very rapidly, during the time necessary to set up the measurement (1−2 min), the FRET efficiency of the mixed sample increased to 0.78, and after 1 h, the value corresponded to the fully mixed coacervates. By confocal microscopy, we however could observe a sample, where each microdroplet already contained both DNAs, but their distribution between different microdroplets was still inhomogeneous (Supplementary Figure S5). This rapid FRET increase occurred without any detectable increase in the size of coacervates, indicating that the mixing occurred mainly by the exchange of DNA molecules between the microdroplets rather than by their physical fusion. To confirm that the microdroplets were in equilibrium with their surrounding phase, a dilution experiment was performed. The dilution of coacervates formed at $R_\pm$ = 1.2 with 10 mM Tris/HCl buffer led to a steep decrease in the normalized turbidity, which achieved a value of 0 at a dilution factor between 2 and 3, which was also confirmed by the total disappearance of the microdroplets in optical microscopy (Supplementary Figure
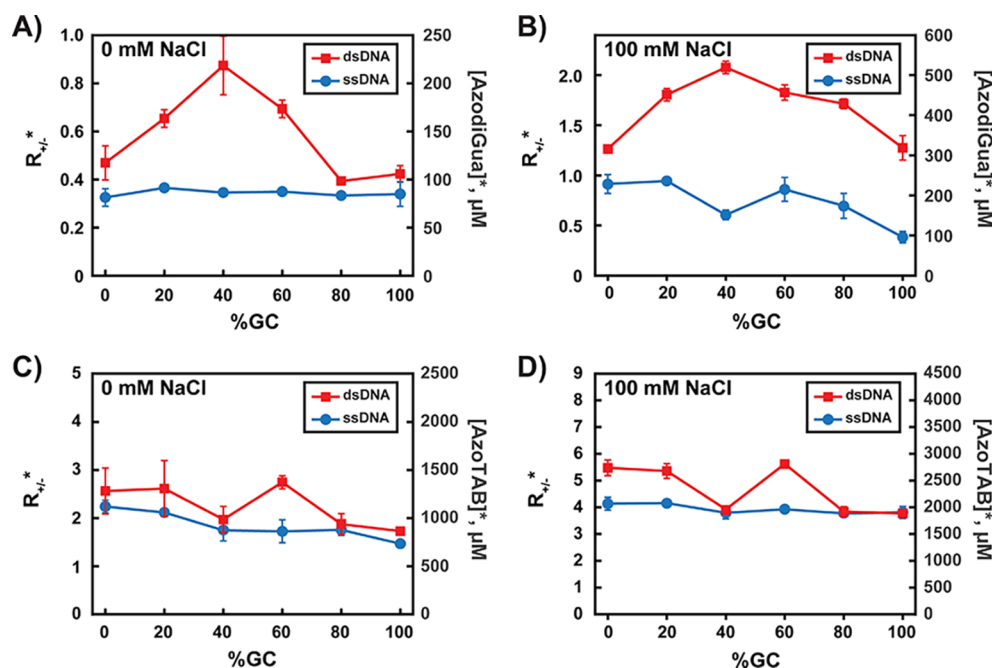
Figure 3. Effect of the sequence on DNA coacervation. Characteristic coacervation concentrations ([AzodiGua]* or [AzoTAB]*) and characteristic charge ratios ($R_\pm^*$) as a function of %GC of DNA for ss- and ds-DNA for AzodiGua (A, B) and AzoTAB (C, D) in the absence (A, C) and presence (B, D) of 100 mM NaCl. [DNA] = 500 μM in charge; 10 mM Tris/HCl, pH 7.4.

S6). This indicated that the system was not kinetically trapped, and a change in the composition resulted in a rapid response of the coacervates.

We then investigated whether AzodiGua would interact differently with ss- and ds-DNA of the same length but different nucleobase compositions (%GC) in the absence and presence of 100 mM NaCl. Turbidity curves systematically showed that (i) more AzodiGua was necessary to induce coacervation at higher ionic strength and (ii) coacervation of ss-DNA occurred at lower concentrations of the intercalator independently on the ionic strength of the solution (Figure 3A,B, Supplementary Figures S7 and S8). In control experiments, we compared these results with DNA coacervation by a monocharged AzoTAB surfactant (Figure 3C,D), as monocationic azobenzenes were shown not to intercalate into the ds-DNA.[33,40] DNA coacervation with AzoTAB occurred at higher charge ratios, and in this case, only a slight difference was observed between the coacervation of ss- and ds-DNA, which can correspond to the weaker charge density and smaller rigidity of the ss-DNA. The observed strong difference in the coacervation of ss- and ds-DNA with AzodiGua thus originated from its intercalative properties. This indicated that intercalation of AzodiGua into ds-DNA did not help in the coacervation, and an excess of the intercalator was necessary to induce coacervation of ds-DNA when intercalation was possible.

We then compared the effect of DNA sequence on the coacervation of ss- and ds-DNA, by using oligonucleotides with the same length but different fractions of GC (%GC). Figure 3A,B shows characteristic $R_\pm^*$ and [AzodiGua]* as a function of %GC in 10 mM Tris/HCl. For ss-DNA, we observed only a slight decrease in [AzodiGua]* (and $R_\pm^*$) as a function of %GC. Interestingly, independent of the salt concentration, bell-shaped curves were found as a function of %GC for ds-DNA. For the coacervation of ds-0%GC-DNA, [AzodiGua]* was only slightly higher than that of ss-DNA;

with increasing %GC, it increased, reached a maximum at 40% GC, and then decreased back for ds-100%GC-DNA. To our knowledge, these results represent the first example of sequence-dependent DNA coacervation by small molecules. To understand this effect of the sequence, we measured binding constants of AzodiGua to the DNA of different %GC (Supplementary Figure S9) and found nonhomogeneous evolution of the binding constant (K_a) as a function of %GC (Supplementary Figure S10). While a similar value of K_a was found for 0%GC and 100%GC ds-DNA (3.10×10^3 and 3.13×10^3 M^{-1}, respectively), a two times higher binding constant was measured for ds-40%GC-DNA (6.5×10^3 M^{-1}). These results indicated a stronger binding of the AzodiGua intercalator for mixed GC/AT pairs, correlating well with a weaker coacervation efficiency. In the control experiments with nonintercalating AzoTAB, no evident effect of the DNA sequence was observed (Figures 3C,D). This further confirmed that bell-shaped curves with ds-DNA originated from the AzodiGua intercalation. All of these results demonstrated that intercalation had the effect of delaying the coacervation of ds-DNA by imposing higher concentrations of intercalators to induce DNA coacervation.

In these experiments, we used one arbitrary DNA sequence for each %GC. In addition, we compared [AzodiGua]* for 6 other ds-DNA sequences, each containing 40%GC (Figure S11). Two of these DNAs had 4 separated GC base pairs, two contained 2 separated blocks of 2 GC base pairs, and the other two contained 1 block having 4 consecutive GC base pairs (Supplementary Figure S11A). All of these sequences demonstrated high critical coacervation concentrations with AzodiGua in a rather narrow range between 195 and 230 μM (Supporting Information, Figure S11B). Even though no direct correlation was found between the theoretically calculated ΔG of hybridization and the [AzodiGua]* (Supporting Information, Figure S11C), we observed that both ds-40%GC-DNAs containing a single block of 4 GC base pairs demonstrated the
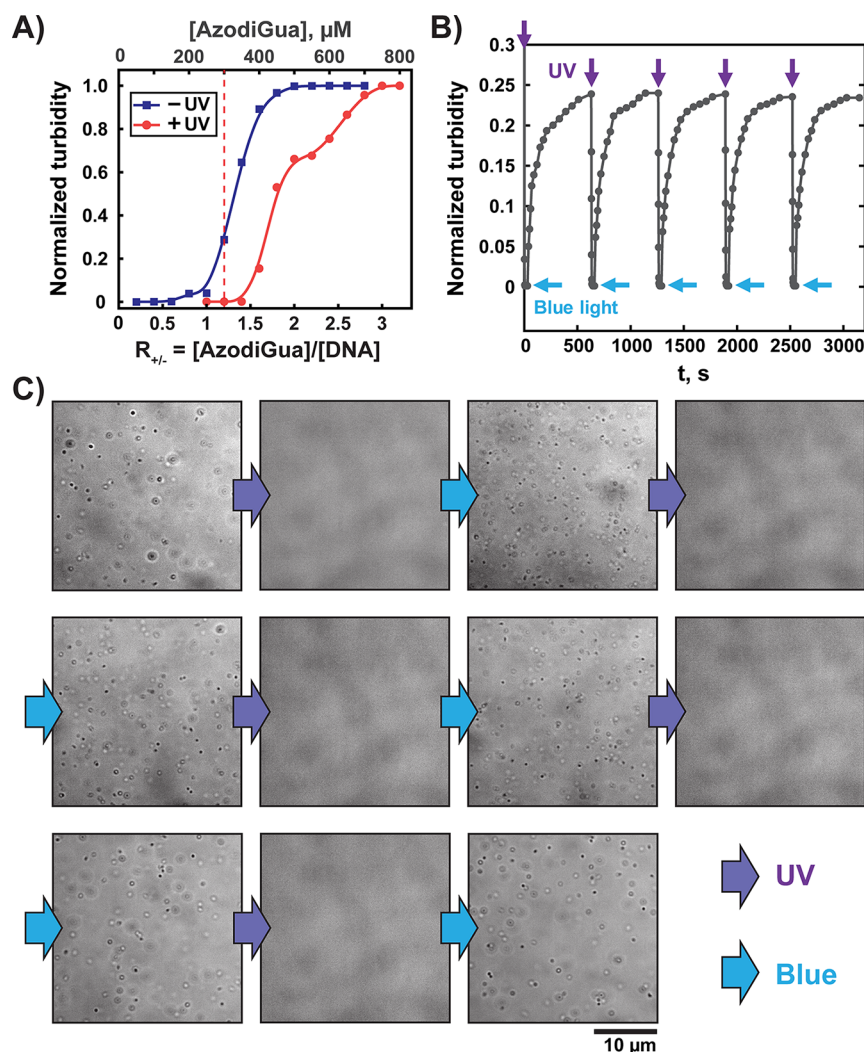
Figure 4. Reversible photocontrol of DNA coacervation. (A) Normalized turbidity as a function of AzodiGua concentrations before and after UV illumination. (B) Five cycles of UV induces dissolution and blue-light-induced reformation of DNA coacervates. (C) Transmission optical microscopy observation of DNA coacervates after consequence cycles of UV (10 s) and blue (10 min) irradiation cycles. All experiments are performed with 500 μM in charge of ds-40%GC-DNA in 10 mM Tris/HCl, pH 7.4. In (B) and (C), [AzodiGua] = 300 μM ($R_\pm$ = 1.2). UV and blue light irradiations were performed at 365 and 440 nm, respectively.

lowest [AzodiGua]*, further confirming that higher AzodiGua amounts are necessary for the coacervation of mixed GC/AT base pairs.

We then studied whether UV-induced photoisomerization of AzodiGua affected the coacervates. First, turbidity curves corresponding to coacervation of ds-40%GC-DNA with AzodiGua before and after UV-induced *trans−cis* isomerization were compared (Figure 4A). Interestingly, *trans−cis* isomerization of AzodiGua led to a shift of turbidity increase from [*trans*-AzodiGua]* = 250 to [*cis*-AzodiGua]* = 350 μM, showing that the *cis*-isomer was less efficient to induce DNA coacervation. Previously, we demonstrated that unlike the *trans*-isomer, *cis*-AzodiGua did not intercalate into DNA.[33] According to the mechanism described above, in which intercalation delays coacervation, one might therefore expect *cis*-AzodiGua to be more efficient for DNA coacervation. Compared to *trans*-AzodiGua, the lower efficiency of DNA coacervation by the *cis*-isomer observed in our experiments can be explained by the shorter distance between its guanidinium groups and its higher polarity, as charged *cis*-azobenzenes are known to exhibit weaker DNA binding and therefore a lower

DNA charge reduction.[21,39] These findings support the conclusion that electrostatic charge neutralization of DNA upon AzodiGua binding is the principal driving force for coacervation in our system.

By fixing the AzodiGua concentration at an intermediate value (300 μM), we applied on the coacervates five consecutive cycles of UV (365 nm) and blue light (440 nm) illumination (Figure 4B). The initial value of turbidity (i.e., absorbance at 700 nm) was normalized to 1. After only 5 s of UV illumination, the normalized turbidity rapidly dropped to 0, showing full photodissolution of DNA coacervate microdroplets, which was confirmed by microscopy observations (Figure 4C). Blue light illumination of the resulting sample for 10 min induced a slower reformation of the microdroplets accompanied by an increase in the normalized turbidity up to 0.24. The strong difference between turbidities of the initial *trans*-AzodiGua solution and samples obtained after blue-light-induced *cis−trans* AzodiGua isomerization can be explained by the lower *trans*-isomer content in the photostationary state. Indeed, freshly prepared solutions of cationic azobenzene derivatives typically contain 100% of *trans*-isomer, whereas in
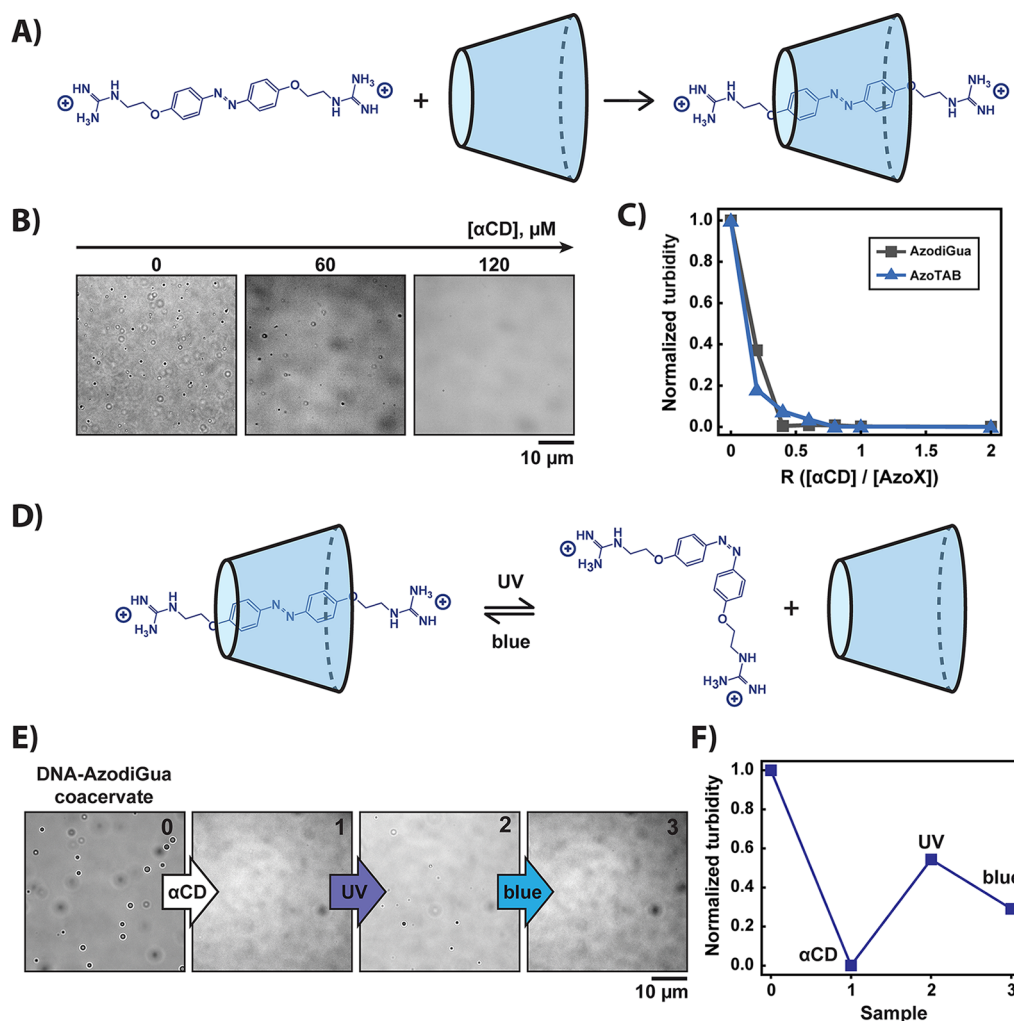
Figure 5. Dissolution and inverse photocontrol of coacervates through host−guest complexation with αCD. (A) Scheme of formation of the *trans*-AzodiGua/αCD inclusion complex. (B) Optical microscopy observation of the dissolution of ds-40%GC-DNA/AzodiGua coacervates ($R_{\pm}$ = 1.2 for 500 μM in charge of DNA) upon addition of αCD. (C) Normalized turbidity of ds-40%GC-DNA coacervates formed with AzodiGua and AzoTAB as a function of αCD concentration, represented by the ratio R = [αCD]/[AzoX]. [ds-40%GC-DNA] = 500 μM in charge; $R_{\pm}$ = 1.2 for both AzodiGua and AzoTAB. (D) Scheme showing the release of *cis*-AzodiGua from αCD upon photoisomerization. (E,F) Optical microscopy (E) and turbidity measurements (F) for inversed photocontrol of DNA coacervation with the AzodiGua/αCD complex; [ds-40%GC-DNA] = 500 μM in charge; [AzodiGua] = 1200 μM; [αCD] = 4800 μM. UV represents a 20 min illumination at 365 nm, and blue corresponds to a 20 min illumination at 440 nm. All experiments are performed in 10 mM Tris/HCl buffer, pH 7.4.

the photostationary state under blue light illumination, the *trans*-AzodiGua content is usually about 75−80%.[41] This cycle was repeated 5 times without any loss of amplitude in the turbidity changes (Figures 4B,C). This demonstrated the photoreversible formation and dissolution of DNA coacervate microdroplets through AzodiGua photoisomerization.

Finally, we applied another approach to dissolve DNA coacervates based on using a host−guest competitor for sequestration of AzodiGua out of the coacervates. For this purpose, we used αCD, whose inclusion complexes with AzodiGua have been very recently characterized.[34] Indeed, AzodiGua efficiently binds to αCD with binding constant K_a = 1.96×10^4 M^{-1} (Figure 5A and Supplementary Figure S12A), which is 3-fold stronger than its binding to ds-40%GC-DNA. First, coacervates were formed in the usual conditions ($R_{\pm}$ = 1.2 for 500 μM of ds-40%GC-DNA). Then, the effect of the αCD addition was followed by optical microscopy (Figure 5B) and turbidity measurements (Figure 5C). Full dissolution of the coacervates occurred upon adding 60 μM of αCD, which

corresponds to the ratio R = [αCD]/[AzodiGua] = 0.4. This indicated that efficient dissolution of the coacervates does not require complexation of all AzodiGua molecules but only necessitates partial sequestration to reach a free AzodiGua concentration below [AzodiGua]*. Similar results have been observed for the dissolution of DNA/AzoTAB coacervates (Figure 5C and Supporting Information, Figure S12B).

As αCD was shown to strongly bind selectively to the *trans*-isomer of AzodiGua,[34] we hypothesized that UV-induced isomerization will release *cis*-AzodiGua from the inclusion complex, making it available for the coacervation of DNA (Figure 5D). In this case, we should find a reversed-photocontrol regime, at which the concentration in AzodiGua is sufficient to promote coacervation in the *cis*-state (UV), and the concentration of αCD is sufficient to dissolve coacervates in the *trans*-state (blue). Such conditions have been found for [AzodiGua] = 1200 μM. In these conditions, adding 4800 μM of αCD induced total dissolution of the coacervates, whereas consequent UV illumination led to reformation of the

coacervates (Figure 5E,F). Following blue light illumination only partially redissolved the coacervates. Even though this process showed limited reversibility, to our knowledge, this result represents the first example of the inverted photocontrol of azobenzenes through the selective sequestration of the *trans*-isomer by CDs.

4. CONCLUSIONS

In conclusion, here, we describe a novel approach for DNA coacervation based on the photosensitive DNA binder AzodiGua. Due to its specific intercalative properties, differences were found in coacervation not only between ss- and ds-DNA but also between ds-DNA having different nucleobase compositions (%GC) or having the same GC content but different distributions of the GC motif. Here, we have limited the study to short oligonucleotides with a fixed length and a limited number of GC contents and distribution. It could be interesting to evaluate the generalizability of the observed findings by systematically studying a broader range of oligonucleotide lengths and sequences, as well as to explore other cationic molecules having different binding modes to DNA, such as minor or major groove binders.

ASSOCIATED CONTENT

Ⓢ Supporting Information

The Supporting Information is available free of charge at https://pubs.acs.org/doi/10.1021/acs.langmuir.5c04489.

> Sequences and names of the used DNA (Table S1); absorbance spectrum of coacervates (Figure S1); turbidity curves for different NaCl concentrations (Figure S2); optical microscopy observation of coacervates after adding SDS and DTAB surfactants (Figure S3); confocal microscopy observation of mixed DNA coacervates (Figure S4) and of the mixture of 2 separately prepared coacervates (Figure S5); effect of dilution on the coacervates (Figure S6); turbidity curves for ss- and ds-DNA of different %GC at 0 mM NaCl (Figure S7) and 100 mM of NaCl (Figure S8); study of AzodiGua binding to ds-DNA of different %GC (Figure S9); AzodiGua/ds-DNA binding constants as a function of the GC content (Figure S10); effect of sequence on the coacervation of different ds-40GC-DNAs (Figure S11); and study of AzodiGua and AzoTAB binding to αCD (Figure S12) (PDF)

AUTHOR INFORMATION

Corresponding Author

Sergii Rudiuk − *CPCV, UMR8228, Department of Chemistry, PSL University, Sorbonne Université, CNRS, Ecole Normale Supérieure, 75005 Paris, France;* ⓘ orcid.org/0000-0003-1728-1163; Email: sergii.rudiuk@ens.psl.eu

Authors

Yunzhe Li − *CPCV, UMR8228, Department of Chemistry, PSL University, Sorbonne Université, CNRS, Ecole Normale Supérieure, 75005 Paris, France*

Julie Pham − *CPCV, UMR8228, Department of Chemistry, PSL University, Sorbonne Université, CNRS, Ecole Normale Supérieure, 75005 Paris, France*

Mathieu Morel − *CPCV, UMR8228, Department of Chemistry, PSL University, Sorbonne Université, CNRS,*

Ecole Normale Supérieure, 75005 Paris, France; ⓘ orcid.org/0000-0002-6284-1708

Damien Baigl − *CPCV, UMR8228, Department of Chemistry, PSL University, Sorbonne Université, CNRS, Ecole Normale Supérieure, 75005 Paris, France;* ⓘ orcid.org/0000-0003-1772-3080

Complete contact information is available at:
https://pubs.acs.org/10.1021/acs.langmuir.5c04489

Notes

The authors declare no competing financial interest.

ACKNOWLEDGMENTS

REFERENCES

(1) Sing, C. E.; Perry, S. L. Recent Progress in the Science of Complex Coacervation. *Soft Matter* **2020**, *16* (12), 2885−2914.

(2) Ban, E.; Kim, A. Coacervates: Recent Developments as Nanostructure Delivery Platforms for Therapeutic Biomolecules. *Int. J. Pharm.* **2022**, *624*, No. 122058.

(3) Yewdall, N. A.; André, A. A. M.; Lu, T.; Spruijt, E. Coacervates as Models of Membraneless Organelles. *Curr. Opin. Colloid Interface Sci.* **2021**, *52*, No. 101416.

(4) Hirose, T.; Ninomiya, K.; Nakagawa, S.; Yamazaki, T. A Guide to Membraneless Organelles and Their Various Roles in Gene Regulation. *Nat. Rev. Mol. Cell Biol.* **2023**, *24* (4), 288−304.

(5) Garabedian, M. V.; Wang, W.; Dabdoub, J. B.; Tong, M.; Caldwell, R. M.; Benman, W.; Schuster, B. S.; Deiters, A.; Good, M. C. Designer Membraneless Organelles Sequester Native Factors for Control of Cell Behavior. *Nat. Chem. Biol.* **2021**, *17* (9), 998−1007.

(6) Chen, Y.; Yuan, M.; Zhang, Y.; Liu, S.; Yang, X.; Wang, K.; Liu, J. Construction of Coacervate-in-Coacervate Multi-Compartment Protocells for Spatial Organization of Enzymatic Reactions. *Chem. Sci.* **2020**, *11* (32), 8617−8625.

(7) Green, C. M.; Sementa, D.; Mathur, D.; Melinger, J. S.; Deshpande, P.; Elbaum-Garfinkle, S.; Medintz, I. L.; Ulijn, R. V.; Díaz, S. A. Sequestration within Peptide Coacervates Improves the Fluorescence Intensity, Kinetics, and Limits of Detection of Dye-Based DNA Biosensors. *Commun. Chem.* **2024**, *7* (1), 49.

(8) Fraccia, T. P.; Martin, N. Non-Enzymatic Oligonucleotide Ligation in Coacervate Protocells Sustains Compartment-Content Coupling. *Nat. Commun.* **2023**, *14* (1), 2606.

(9) Zhang, L.; Chen, M.; Wang, Z.; Zhong, M.; Chen, H.; Li, T.; Wang, L.; Zhao, Z.; Zhang, X.-B.; Ke, G.; Liu, Y.; Tan, W. Spatiotemporal Regulation of Cell Fate in Living Systems Using Photoactivatable Artificial DNA Membraneless Organelles. *ACS Cent. Sci.* **2024**, *10* (6), 1201−1210.

(10) Erkamp, N. A.; Verwiel, M. A. M.; Qian, D.; Sneideris, T.; Spaepen, F. A.; Weitz, D. A.; van Hest, J. C. M.; Knowles, T. P. J. Biomolecular Condensates with Complex Architectures via Controlled Nucleation. *Nat. Chem. Eng.* **2024**, *1* (6), 430−439.

(11) Forenzo, C.; Larsen, J. Complex Coacervates as a Promising Vehicle for mRNA Delivery: A Comprehensive Review of Recent Advances and Challenges. *Mol. Pharmaceutics* **2023**, *20* (9), 4387−4403.

(12) Nasr, S. S.; Lee, S.; Thiyagarajan, D.; Boese, A.; Loretz, B.; Lehr, C.-M. Co-Delivery of mRNA and pDNA Using Thermally

Stabilized Coacervate-Based Core-Shell Nanosystems. *Pharmaceutics* **2021**, *13* (11), No. 1924.

(13) Wang, C.; You, J.; Gao, M.; Zhang, P.; Xu, G.; Dou, H. Bio-Inspired Gene Carriers with Low Cytotoxicity Constructed Via The Assembly of Dextran Nanogels and Nano-Coacervates. *Nanomedicine* **2020**, *15* (13), 1285−1296.

(14) Sun, Y.; Lau, S. Y.; Lim, Z. W.; Chang, S. C.; Ghadessy, F.; Partridge, A.; Miserez, A. Phase-Separating Peptides for Direct Cytosolic Delivery and Redox-Activated Release of Macromolecular Therapeutics. *Nat. Chem.* **2022**, *14* (3), 274−283.

(15) Last, M. G. F.; Deshpande, S.; Dekker, C. pH-Controlled Coacervate-Membrane Interactions within Liposomes. *ACS Nano* **2020**, *14* (4), 4487−4498.

(16) Wee, W. A.; Sugiyama, H.; Park, S. Photoswitchable Single-Stranded DNA-Peptide Coacervate Formation as a Dynamic System for Reaction Control. *iScience* **2021**, *24* (12), No. 103455.

(17) Martin, N.; Tian, L.; Spencer, D.; Coutable-Pennarun, A.; Anderson, J. L. R.; Mann, S. Photoswitchable Phase Separation and Oligonucleotide Trafficking in DNA Coacervate Microdroplets. *Angew. Chemie Int. Ed.* **2019**, *58* (41), 14594−14598.

(18) Lafon, S.; Martin, N. Reversible Photocontrol of DNA Coacervation. *Methods Enzymol.* **2021**, *646*, 329−351.

(19) Diguet, A.; Mani, N. K.; Geoffroy, M.; Sollogoub, M.; Baigl, D. Photosensitive Surfactants with Various Hydrophobic Tail Lengths for the Photocontrol of Genomic DNA Conformation with Improved Efficiency. *Chem.−Eur. J.* **2010**, *16* (39), 11890−11896.

(20) Rudiuk, S.; Yoshikawa, K.; Baigl, D. Enhancement of DNA Compaction by Negatively Charged Nanoparticles. Application to Reversible Photocontrol of DNA Higher-Order Structure. *Soft Matter* **2011**, *7* (12), 5854.

(21) Estévez-Torres, A.; Crozatier, C.; Diguet, A.; Hara, T.; Saito, H.; Yoshikawa, K.; Baigl, D. Sequence-Independent and Reversible Photocontrol of Transcription/Expression Systems Using a Photosensitive Nucleic Acid Binder. *Proc. Natl. Acad. Sci. U. S. A.* **2009**, *106* (30), 12219−12223.

(22) Rudiuk, S.; Saito, H.; Hara, T.; Inoue, T.; Yoshikawa, K.; Baigl, D. Light-Regulated mRNA Condensation by a Photosensitive Surfactant Works as a Series Photoswitch of Translation Activity in the Presence of Small RNAs. *Biomacromolecules* **2011**, *12* (11), 3945−3951.

(23) Sato, Y.; Sakamoto, T.; Takinoue, M. Sequence-Based Engineering of Dynamic Functions of Micrometer-Sized DNA Droplets. *Sci. Adv.* **2020**, *6* (23), No. eaba3471.

(24) Gong, J.; Tsumura, N.; Sato, Y.; Takinoue, M. Computational DNA Droplets Recognizing miRNA Sequence Inputs Based on Liquid-Liquid Phase Separation. *Adv. Funct. Mater.* **2022**, *32*, No. 2202322.

(25) Liu, W.; Deng, J.; Song, S.; Sethi, S.; Walther, A. A Facile DNA Coacervate Platform for Engineering Wetting, Engulfment, Fusion and Transient Behavior. *Commun. Chem.* **2024**, *7* (1), 100.

(26) Agarwal, S.; Osmanovic, D.; Dizani, M.; Klocke, M. A.; Franco, E. Dynamic Control of DNA Condensation. *Nat. Commun.* **2024**, *15* (1), 1915.

(27) Chang, L.-W.; Lytle, T. K.; Radhakrishna, M.; Madinya, J. J.; Vélez, J.; Sing, C. E.; Perry, S. L. Sequence and Entropy-Based Control of Complex Coacervates. *Nat. Commun.* **2017**, *8* (1), 1273.

(28) Lebold, K. M.; Best, R. B. Tuning Formation of Protein−DNA Coacervates by Sequence and Environment. *J. Phys. Chem. B* **2022**, *126* (12), 2407−2419.

(29) Pak, C. W.; Kosno, M.; Holehouse, A. S.; Padrick, S. B.; Mittal, A.; Ali, R.; Yunus, A. A.; Liu, D. R.; Pappu, R. V.; Rosen, M. K. Sequence Determinants of Intracellular Phase Separation by Complex Coacervation of a Disordered Protein. *Mol. Cell* **2016**, *63* (1), 72−85.

(30) Vieregg, J. R.; Lueckheide, M.; Marciel, A. B.; Leon, L.; Bologna, A. J.; Rivera, J. R.; Tirrell, M. V. Oligonucleotide-Peptide Complexes: Phase Control by Hybridization. *J. Am. Chem. Soc.* **2018**, *140* (5), 1632−1638.

(31) Sun, J. S.; François, J. C.; Montenay-Garestier, T.; Saison-Behmoaras, T.; Roig, V.; Thuong, N. T.; Hélène, C. Sequence-Specific Intercalating Agents: Intercalation at Specific Sequences on Duplex DNA via Major Groove Recognition by Oligonucleotide-Intercalator Conjugates. *Proc. Natl. Acad. Sci. U. S. A.* **1989**, *86* (23), 9198−9202.

(32) Jolley, E. A.; Hardebeck, L. K. E.; Ren, Y.; Adams, M. S.; Lewis, M.; Znosko, B. M. The Effects of Varying the Substituent and DNA Sequence on the Stability of 4-Substituted DNA-Naphthalimide Complexes. *Biophys. Chem.* **2018**, *239* (April), 29−37.

(33) Bergen, A.; Rudiuk, S.; Morel, M.; Le Saux, T.; Ihmels, H.; Baigl, D. Photodependent Melting of Unmodified DNA Using a Photosensitive Intercalator: A New and Generic Tool for Photo-reversible Assembly of DNA Nanostructures at Constant Temperature. *Nano Lett.* **2016**, *16* (1), 773−780.

(34) Abodja, O.; Walrant, A.; Rudiuk, S.; Morel, M.; Baigl, D. Azobenzene DNA Intercalator/Cyclodextrin Pseudo-Rotaxane: From Photoswitchable Chirality and Fluorescence to DNA Melting Control. *ChemistryOpen* **2025**, *00*, No. e202500382.

(35) Zhou, L.; Retailleau, P.; Morel, M.; Rudiuk, S.; Baigl, D. Photoswitchable Fluorescent Crystals Obtained by the Photo-reversible Coassembly of a Nucleobase and an Azobenzene Intercalator. *J. Am. Chem. Soc.* **2019**, *141* (23), 9321−9329.

(36) Abodja, O.; Touati, N.; Morel, M.; Rudiuk, S.; Baigl, D. ATP/Azobenzene-Guanidinium Self-Assembly into Fluorescent and Multi-Stimuli-Responsive Supramolecular Aggregates. *Commun. Chem.* **2024**, *7* (1), 142.

(37) Estévez-Torres, A.; Baigl, D. DNA Compaction: Fundamentals and Applications. *Soft Matter* **2011**, *7* (15), 6746.

(38) Rudiuk, S.; Yoshikawa, K.; Baigl, D. Enhancement of DNA Compaction by Negatively Charged Nanoparticles: Effect of Nano-particle Size and Surfactant Chain Length. *J. Colloid Interface Sci.* **2012**, *368* (1), 372−377.

(39) Venancio-Marques, A.; Bergen, A.; Rossi-Gendron, C.; Rudiuk, S.; Baigl, D. Photosensitive Polyamines for High-Performance Photocontrol of DNA Higher-Order Structure. *ACS Nano* **2014**, *8* (4), 3654−3663.

(40) Le Ny, A.-L. M.; Lee, C. T. Conformation and Dynamics of DNA Molecules during Photoreversible Condensation. *Biophys. Chem.* **2009**, *142* (1−3), 76−83.

(41) Heller, H. G. Photochromic Materials (Organic). In *Encyclopedia of Materials: Science and Technology*; Elsevier, 2001; pp 6904−6909.